Du et al. *Zool. Res.* 2024, 45(6): 1276−1286
https://doi.org/10.24272/j.issn.2095-8137.2024.173
https://cstr.cn/32248.14.zr.2024.173

ZR | Zoological Research

Article Open Access

# Integrative cross-species transcriptome analysis reveals earlier occurrence of myelopoiesis in pre-circulation primates compared to mice

Junjie Du[1,2,#], Zongcheng Li[2,#], Yandong Gong[2,#], Yu Lan[3,*], Bing Liu[1,2,*]

[1] *Chinese PLA Medical School*, *Chinese PLA General Hospital*, *Beijing* 100853, *China*

[2] *State Key Laboratory of Experimental Hematology*, *Haihe Laboratory of Cell Ecosystem*, *Senior Department of Hematology*, *Fifth Medical Center of Chinese PLA General Hospital*, *Beijing* 100071, *China*

[3] *Key Laboratory for Regenerative Medicine of Ministry of Education*, *Institute of Hematology*, *School of Medicine*, *Jinan University*, *Guangzhou*, *Guangdong* 510632, *China*

## ABSTRACT

Hematopoiesis originates in the yolk sac, which forms prior to the establishment of blood circulation and exhibits distinct developmental processes between primates and mice. Despite increasing appreciation of yolk sac hematopoiesis for its lifelong contribution to the adult hematopoietic system and its regulatory roles in organogenesis, cross-species differences, particularly before the onset of blood circulation, remain incompletely understood. In this study, we constructed an integrative cross-species transcriptome atlas of pre-circulation hematopoiesis in humans, monkeys (*Macaca fascicularis*), and mice. This analysis identified conserved populations between primates and mice, while also revealing more differentiated myeloid, erythroid, and megakaryocytic lineages in pre-circulation primates compared to mice. Specifically, *SPP1*-expressing macrophages were detected in primates before the onset of blood circulation but were absent in mice. Cell-cell communication analysis identified *CSF1*$^{+}$ extraembryonic mesoderm cells as a potential supportive niche for macrophage generation, with ligand-receptor interactions between macrophages and other cell populations in the human yolk sac. Interestingly, pre-circulation *SPP1*$^{+}$ macrophages exhibited hallmark signatures reminiscent of a macrophage subset that positively regulates hematopoietic stem cell generation. Our findings provide a valuable cross-species resource, advancing our understanding of human pre-circulation yolk sac hematopoiesis and offering a theoretical basis for the regeneration of functional blood cells.



**Keywords:** Yolk sac; Hematopoiesis; Macrophage; Integrative analysis; Single-cell RNA sequencing

## INTRODUCTION

The first wave of hematopoiesis occurs in the yolk sac within structures known as blood islands, which are derived from mesoderm precursors during gastrulation preceding the establishment of blood circulation (Dzierzak & Bigas, 2018). In mice, the earliest yolk sac hematopoiesis, also referred as primitive hematopoiesis, generates primitive erythroid cells, macrophages, and megakaryocytes (Mk) from embryonic day (E) 7.5 (Palis, 2016; Palis et al., 2010). After blood circulation begins at approximately E8.25, a definitive wave of yolk sac hematopoiesis produces erythroid-myeloid progenitor (EMP) cells (Canu & Ruhrberg, 2021). Hematopoietic stem cells (HSCs), with capacity for self-renewal and multi-lineage reconstitution, arise from hemogenic endothelial cells (HECs) within the dorsal aorta of the aorta-gonad-mesonephros (AGM) region at E10.5 (Medvinsky & Dzierzak, 1996). Emerging evidence has demonstrated that yolk sac hematopoiesis contributes to adult hematopoiesis throughout life and plays a regulatory role in organ development (Ginhoux et al., 2010; Monticelli et al., 2024; Neo et al., 2021). Embryonic hematopoiesis was considered to be largely conserved among mammals in terms of spatiotemporal and molecular dynamics. In humans, primitive erythroblasts surrounded by endothelium are visible in the yolk sac as early as Carnegie Stage 6 (CS6) before the onset of blood circulation (21 days post-fertilization, CS10) (Peschle et al.,

Received: 23 May 2024; Accepted: 19 June 2024; Online: 20 June 2024

Foundation items: This work was supported by the Beijing Natural Science Foundation (5222035), Beijing Nova Program (Z211100002121033, 20230484407), National Key R&D Program of China (2021YFA0805703, 2021YFA1100901, 2022YFA1105700), National Natural Science Foundation of China (31930054, 32100646, 82370107, 82270118), and Program for Guangdong Introducing Innovative and Entrepreneurial Teams (2017ZT07S347)

[#]Authors contributed equally to this work

*Corresponding authors, E-mail: rainyblue_1999@126.com; bingliu17@yahoo.com

1984). However, despite growing interest, insights into human yolk sac hematopoiesis are limited due to the scarcity of early human embryos and the lack of robust methods to capture and validate rare cell populations during yolk sac hematopoiesis, especially for hematopoietic events prior to circulation onset. While our current knowledge of its role in human development has been substantially informed by studies in non-human model systems, such as mice and non-human primates (e.g., *Macaca fascicularis*, hereafter abbreviated as monkey) (Zhang et al., 2022), cross-species differences have emerged within the critical window of yolk sac hematopoiesis. For instance, the yolk sac itself develops differently between humans and mice in terms of its spatial relationship to the embryo body. In humans, it develops in front of the embryo, resembling a balloon, and follows a two-phase developmental pattern involving the primary and secondary yolk sacs. In contrast, the mouse yolk sac surrounds the embryo body and undergoes a single-stage development (Ross & Boroviak, 2020). These developmental distinctions underscore the importance of recognizing both the similarities and differences in yolk sac hematopoiesis across species (Goh et al., 2023).

Single-cell genomics has facilitated our understanding of hematopoiesis development, providing unprecedented resolution and bridging the cross-species gap. Despite cross-species cellular correspondence, human yolk sac-derived myeloid progenitors (YSMP), identified at single-cell level, demonstrate myeloid-biased multi-lineage potential, while mouse EMP show both erythroid and myeloid potential in culture (Bian et al., 2020). However, single-cell transcriptome comparisons of pre-circulation hematopoiesis in humans, monkeys (heart activity begins at approximately 21 days, CS10), and mice are still lacking.

In this study, we performed a cross-species integrative analysis of single-cell RNA sequencing (scRNA-seq) data from hematopoietic cell populations before the onset of circulation in humans (Tyser et al., 2021), monkeys (*in vivo* and *in vitro*) (Gong et al., 2023; Zhai et al., 2022), and mice (Pijuan-Sala et al., 2019). Our analysis identified conserved cellular populations across species, as well as the earlier occurrence of myelopoiesis in pre-circulation primates compared to mice. These findings provide a deeper understanding of conserved and divergent features of pre-circulation hematopoiesis across species, helping to bridge the interspecies knowledge gap.

## MATERIALS AND METHODS

### Data collection and quality control

To construct a comprehensive cross-species transcriptome atlas of early yolk sac hematopoiesis, we collected scRNA-seq datasets from human, monkey (both *in vivo* and *in vitro*), and mouse studies, drawing on four key published works. Specifically, raw count matrices and cell information were sourced from studies on human gastrulation at CS7 (Tyser et al., 2021), monkey gastrulation and early organogenesis (Zhai et al., 2022), monkey embryo embedded 3D culture (Gong et al., 2023), and mouse gastrulation (Pijuan-Sala et al., 2019).

To ensure the reliability of the integrative datasets, we applied basic pre-processing and quality control standards consistent with those detailed in the original publications, which had already provided high-quality, publication-level scRNA-seq expression matrices. For humans, sequencing was performed using the Smart-seq2 protocol (Picelli et al., 2014), with reads aligned to the GRCh38 reference genome. The datasets from monkeys (*in vivo* and *in vitro*) and mice were sequenced using the 10× Genomics Chromium platform, with monkey data aligned to the *Macaca fascicularis* 5.0 genome and mouse data to GRCm38 (v.92).

Given the varied throughput capacities of the Smart-seq2 and 10× Genomics platforms, we down-sampled the monkey (*in vivo* and *in vitro*) and mouse datasets by stratified sampling based on cell population annotations from the original articles. In total, 573 cells (median read count: 335 163) from the human dataset, 1 155 cells (median unique molecular identifier (UMI): 8 230, original cell size: 5 931) from the monkey *in vivo* dataset, 1 035 cells (median UMI: 16 236, original cell size: 2 953) from the monkey *in vitro* dataset, and 1 057 cells (median UMI: 11 338, original cell size: 15 875) from the mouse dataset were retained for downstream analyses.

### Cross-species homologous gene conversion

To identify homologous genes across species, the “useMart” and “getLDS” functions in the biomaRt package (v.2.54.1) (Durinck et al., 2009) were used to download gene symbols and generate a reference set of homologous genes. For the integration of cross-species scRNA-seq datasets, only homologous genes shared among all three species were retained for downstream analysis, yielding a total of 13 549 shared genes. The proportion of these shared homologous genes among the top 3 000 highly variable genes in individual species analyses was 70.8% in humans, 83.9% in mice, and 78.4% and 73.4% in monkeys (*in vivo* and *in vitro*, respectively). For integration, homologous genes in the monkey and mouse datasets were converted to their corresponding human homologs.

### Re-annotation of cell clusters from human and monkey (*in vivo*) datasets

To ensure comparable resolution in the identification of critical cell populations across the four datasets, re-annotation of cell clusters in the human and monkey (*in vivo*) datasets was performed. The Seurat package (v.4.3.0) (Hao et al., 2021) in R was used for fundamental processing and analysis, including scRNA-seq count matrix transformation, normalization, dimensionality reduction, and visualization. For the human dataset, unsupervised clustering was performed using the “FindClusters” function in Seurat, with the resolution parameter set to 2. In the monkey (*in vivo*) dataset, batch effects were corrected using the “RunFastMNN” function in the SeuratWrappers package (v.0.3.0). Dimensionality reduction was achieved through uniform manifold approximation and projection (UMAP) using the top 20 mutual nearest neighbor (MNN) dimensions. Unsupervised clustering of the monkey (*in vivo*) dataset was performed using the “FindClusters” function at a resolution at 0.5.

### Integration and dimensionality reduction of cross-species datasets

To correct batch effects among the cross-species datasets, an anchor-based approach within the Seurat package was applied. First, “SCTransform” was used with variable.features n set to 3 000 for each dataset. The identified anchor feature genes, along with the top 30 dimensions from canonical correlation analysis, were used for “FindIntegrationAnchors”,

with k.weight set to 150 in the "IntegrateData" function. Dimensionality reduction was then performed using the "RunPCA" function, with the top 30 principal components employed for subsequent dimensionality reduction through the RunUMAP procedure.

**Correlation analysis and hierarchical clustering**

To investigate the transcriptomic relationships between cluster populations across the four datasets, Pearson correlation analysis was performed using the top 20 principal components derived from the integrated dataset. Hierarchical clustering was subsequently performed based on the Pearson correlation coefficients between each pair of cell populations using "stats" packages in R (v.4.2.3).

**Differentially expressed genes (DEGs)**

To identify DEGs cross multiple clusters, the "FindAllMarkers" function in Seurat was applied. Expression values were transformed using log(TPM/100+1), and the Wilcoxon rank-sum test ("wilcox" method) was used to assess significance. Only genes expressed in a minimum fraction of 0.1 cells in either population were included, with "pseudocount.use" set to 0.1. Only genes that met certain criteria (fold-change≥2 and $P$≤0.05) were retained as DEGs.

**Signature score analysis**

To calculate signature scores of hematopoietic progenitors in the human and monkey (*in vivo* and *in vitro*) datasets, the top 60 DEGs between mouse blood progenitors (BP) and EMP were used as input. Signature scores were computed using the "addModuleScore" function in the Seurat package.

**Trajectory analysis using monocle3**

The Monocle3 package (v.1.3.1) (Cao et al., 2019) was employed to predict developmental trajectories and calculate pseudotime, using default parameters. Initially, the coordinates and cluster assignments of each cell were aligned with the original UMAP from the integrated cross-species datasets. A principal graph was then fitted using the "learn_graph" function, followed by cell ordering along the pseudotime trajectory using the "Order_cells" function, where mesoderm progenitor cells across all four datasets were designated as root cells. The pseudotime trajectory was then visualized with the "plot_cells" function. In hematopoietic cell populations, three primary trajectories were predicted, corresponding to the differentiation pathways of myeloid, Mk, and erythroid cell populations. To further analyze species-specific distributions along the pseudotime trajectory, a ridge plot visualization was generated. The common starting node for all three predicted trajectories was designated as the "Root" point for the ridge plot. Specifically, the shared part of the trajectory was analyzed for both the myeloid and Mk trajectories.

**Cell-cell interaction predictions using CellChat**

To assign putative cell-cell interactions within yolk sac clusters (based on original sampling) in the CS7 human dataset, CellChat (v.1.6.1) was used (Jin et al., 2021). First, a log-transformed and normalized gene expression matrix for all cell clusters was prepared, and the human ligand-receptor interaction database was applied to analyze potential cell-cell interactions. The probability of cell-cell communication between any interacting cell groups was calculated using the "computeCommunProb" function, with k.min set to 5. Weak interactions were filtered out using the "filterCommunication" function, with min.cells set to 3. Communication probabilities at the signaling pathway level were then computed using the "computeCommunProbPathway" function. The "netVisual_circle" function was then used to visualize the scaled strength of the cell-cell communication networks. The general communication patterns of incoming and outgoing signals were predicted using the "identifyCommunicationPatterns" function, with $k$=3. Subsequently, the "netAnalysis_computeCentrality" and "netAnalysis_signalingRole_network" functions were applied to determine the importance scores of cell populations as dominant senders, receivers, mediators, and influencers in the intercellular communication network. Finally, the "netVisual_bubble" function was used to visualize significant ligand-receptor interactions between cell populations.

**Differentiation state predictions using CytoTRACE**

CytoTRACE (v.0.3.3) (Gulati et al., 2020) was used to predict the differentiation state of two subsets of the extraembryonic mesoderm cell population. The raw count matrix of the relevant cell populations was used as input into the "CytoTRACE" function with default settings to predict the rank cells by their differentiation states.

**Gene set variation analysis (GSVA)**

To assess the expression levels of proinflammatory signaling pathways across cell clusters in the human CS7 embryo, the "gsva" function in the GSVA package (v.1.48.2) was applied (Hänzelmann et al., 2013), with the parameter method=ssgsea. Proinflammatory-related gene sets were collected from the Human MSigDB Collections (https://www.gsea-msigdb.org/gsea/msigdb/collections.jsp). Visualization of the results was performed using the pheatmap package in R (v.1.0.12, https://github.com/raivokolde/pheatmap).

**Statistical analysis**

All statistical analyses were conducted using R software. The two-sample Wilcoxon rank-sum test was employed to compare transcript counts, gene expression levels, and feature scores between two cell clusters. Further details regarding statistical analysis are described above. Most plots were generated using the ggplot2 package (v.3.5.1, https://ggplot2.tidyverse.org), unless otherwise specified.

**Pooled scRNA-seq data and code availability**

The pooled cross-species scRNA-seq count matrix and custom R code for data analysis and visualization are available in a public repository (https://github.com/Liu-Lan-lab/Project_cross-species_pre-circulation_hematopoiesis). Additional codes are available upon request.

## RESULTS

**Construction of integrative cross-species transcriptome atlas of pre-circulation hematopoiesis**

For integrative analysis of pre-circulation hematopoiesis across species, we collected corresponding scRNA-seq datasets from humans (CS7) (Tyser et al., 2021), monkeys (CS8–CS9 for *in vivo* and 18–25 days post-fertilization for *in vitro*) (Gong et al., 2023; Zhai et al., 2022), and mice (E6.5–E8.5) (Pijuan-Sala et al., 2019). These datasets included mesoderm precursor, endothelial, and hematopoietic cells. Additionally, post-circulation hematopoietic populations from E8.25 to E8.5 in mice, including EMP from the definitive wave of yolk sac hematopoiesis, were included as a reference

for identifying corresponding populations in primates (Figure 1A).

Before integration, we re-annotated the hematopoietic-related cell clusters in the human and monkey (*in vivo*) datasets. For the human CS7 embryo, emerging mesoderm cells, advanced mesoderm cells, extraembryonic mesoderm (ExM) cells, haemato-endothelial progenitors, and erythroblasts (Ery), as defined in the original study, were included for downstream analysis (Figure 1B) (Tyser et al., 2021). The haemato-endothelial progenitors were further refined into five clusters, including endothelial cells (EC; expressing *CDH5*), hematopoietic progenitor cells (HPC; expressing *SPINK2*, *CD34*, and *MYB*), megakaryocyte progenitors (MkP; expressing *ITGA2B* and *PF4*), myeloid progenitors (MyP; expressing *MPO* and *AZU1*), macrophages (Mac; expressing *CD68*, *C1QA*, and *C1QC*) (Figure 1B, C) based on signature genes. In the monkey *in vivo* dataset, we performed unsupervised clustering analysis of populations originally labeled as EC and hematopoietic cells (blood progenitors, BP; Mac; and erythrocytes, Ery) and reclassified them into nine subclusters (Figure 1D). Hemogenic angioblasts (HABs), expressing both mesoderm genes, such as *ETV2* and *KDR*, and hematopoietic genes, such as *TAL1* (also known as SCL), were identified as shared precursors of endothelial and hematopoietic lineages (Figure 1E). In the hematopoietic lineage, HEC, characterized by *KCNK17*, *RUNX1*, and *GFI1* expression, were also detected (Figure 1D, E) (Calvanese et al., 2022; Goh et al., 2023). Additionally, two distinct HPC subsets were identified (Figure 1D): HPC1 was clustered with MkP and Ery and expressed *ITGA2B* (encodes CD41) and *GATA1* (Figure 1D, E), while HPC2 expressed *CD34* and *SPI1* and clustered with MyP (*MPO*) and Mac (*C1QC*), indicating myeloid-biased molecular characteristics (Figure 1D, E). The identification of these two HPC subsets, one with erythroid and megakaryocytic features and the other with myeloid features, in the monkey (*in vivo*) pre-circulation dataset was consistent with the previous monkey *in vitro* study (Gong et al., 2023). In addition, the cell annotations from the monkey (*in vitro*) and mouse datasets, as defined in their original publications, were retained for downstream analysis.

Homologous genes from the monkey and mouse datasets were transformed to their corresponding human homologs for cross-species integration. To ensure comparability in cell number size, the monkey and mouse datasets were down-sampled. In total, 3 820 cells were included in the downstream analysis. After cross-species batch correction and dimensionality reduction, UMAP visualization grouped the cross-species datasets into four major categories, including *POU5F1*- (also known as OCT4) and *KDR*-expressing mesoderm precursors, ExM cells (defined by the mesenchymal gene *POSTN*), endothelial cells, and hematopoietic clusters. Within the hematopoietic clusters, cells were distributed along differentiation paths defined by signature genes for hematopoietic progenitor (*CD34*), erythroid (*GATA1* and *HBZ*), Mk (*GP9*), and myeloid cells (*SPI1* and *CSF1R*; Figure 1F–I). Notably, a subset of mouse yolk sac EC (YSEC) clustered with monkey HEC and hematopoietic populations, reflecting their close association with hematopoiesis, and thus were designated as mouse HEC (Figure 1G) (Pijuan-Sala et al., 2019; Wang et al., 2021).

Taken together, we construct a cross-species transcriptome atlas of pre-circulation yolk sac hematopoiesis in humans, monkeys (*in vivo* and *in vitro*), and mice (Figure 1F, G), characterizing the molecular features of mesodermal precursors to hematopoietic, endothelial, and mesenchymal populations.

**Earlier myelopoiesis in primates compared to mice before blood circulation onset**

While two sequential waves of yolk sac hematopoiesis are well-characterized in mice, the corresponding process in primates remains less established. To explore interspecies cellular similarities during early yolk sac hematopoiesis, we performed correlation analysis and hierarchical clustering (Figure 2A). Six of the nine hierarchical clusters identified were hematopoietic-related, including hemogenic endothelial, hematopoietic progenitor, myeloid, Mk, and Ery cells (Figure 2A). Notably, BP (blood progenitors 1 and 2 described in Pijuan-Sala et al. (2019)), the hematopoietic progenitors of primitive hematopoiesis in the mouse yolk sac, clustered with monkey HPC1 (both *in vivo* and *in vitro*), while human HPC were closely aligned with monkey HPC2 (both *in vivo* and *in vitro*), which expressed myeloid-biased signatures (Figure 2A). Additionally, the mouse EMP clustered with myeloid progenitor populations from both human and monkey datasets (Figure 2A), with EMP showing a stronger Pearson correlation with human HPC and monkey HPC2 (*in vivo* and *in vitro*) compared to monkey HPC1 (*in vivo* and *in vitro*) (Figure 2A). Signature score analysis based on signature genes from mouse BP and EMP further confirmed the similarity between monkey HPC1 and mouse BP, as well as between human HPC and monkey HPC2 with mouse EMP (Figure 2B).

Yolk sac-derived hematopoietic progenitors differentiate into multi-lineage progeny either *in situ* or following migration to other hematopoietic niches. However, it is unclear whether significant interspecies differences exist in the differentiation states of yolk sac hematopoiesis before blood circulation begins. Leveraging the cross-species transcriptome atlas, we systematically assessed the differentiation states of the hematopoietic lineages across species. Our reconstruction of differentiation trajectories predicted three putative pathways, including myeloid, megakaryocytic, and erythroid lineages (Figure 2C). Further evaluation of cross-species distributions (*in vivo* data only) along these trajectories revealed that pre-circulation mouse cells were generally more undifferentiated compared to those from primates in all three trajectories (Figure 2D). Remarkably, primate pre-circulation embryos (CS7–CS9) exhibited more advanced differentiation states in the myeloid trajectory than mouse post-circulation hematopoiesis until E8.5 (Figure 2D). These results suggest that myeloid, megakaryocytic, and erythroid differentiation progresses more rapidly in primates than in mice before circulation onset. DEG analysis of myeloid-biased progenitors between primates (human HPC and monkey (*in vivo*) HPC2) and mice (EMP) revealed higher expression of pre-macrophage signature genes (e.g., *TYMP, PTGS2*, and *CD52*) in primates compared to mice (Figure 2E) (Goh et al., 2023; Mass et al., 2016). In addition, *S100A4*, a known macrophage regulator, was exclusively expressed in primate hematopoietic progenitors (Figure 2E) (Li et al., 2010). In contrast, mouse progenitors showed greater expression of common myeloid progenitor (*RPS6*) and promonocyte (*CST3*) markers (Goh et al., 2023) (Figure 2E). Given that pre-macrophages represent an intermediate state between progenitors and mature macrophages, these results further indicate more advanced myeloid differentiation in pre-

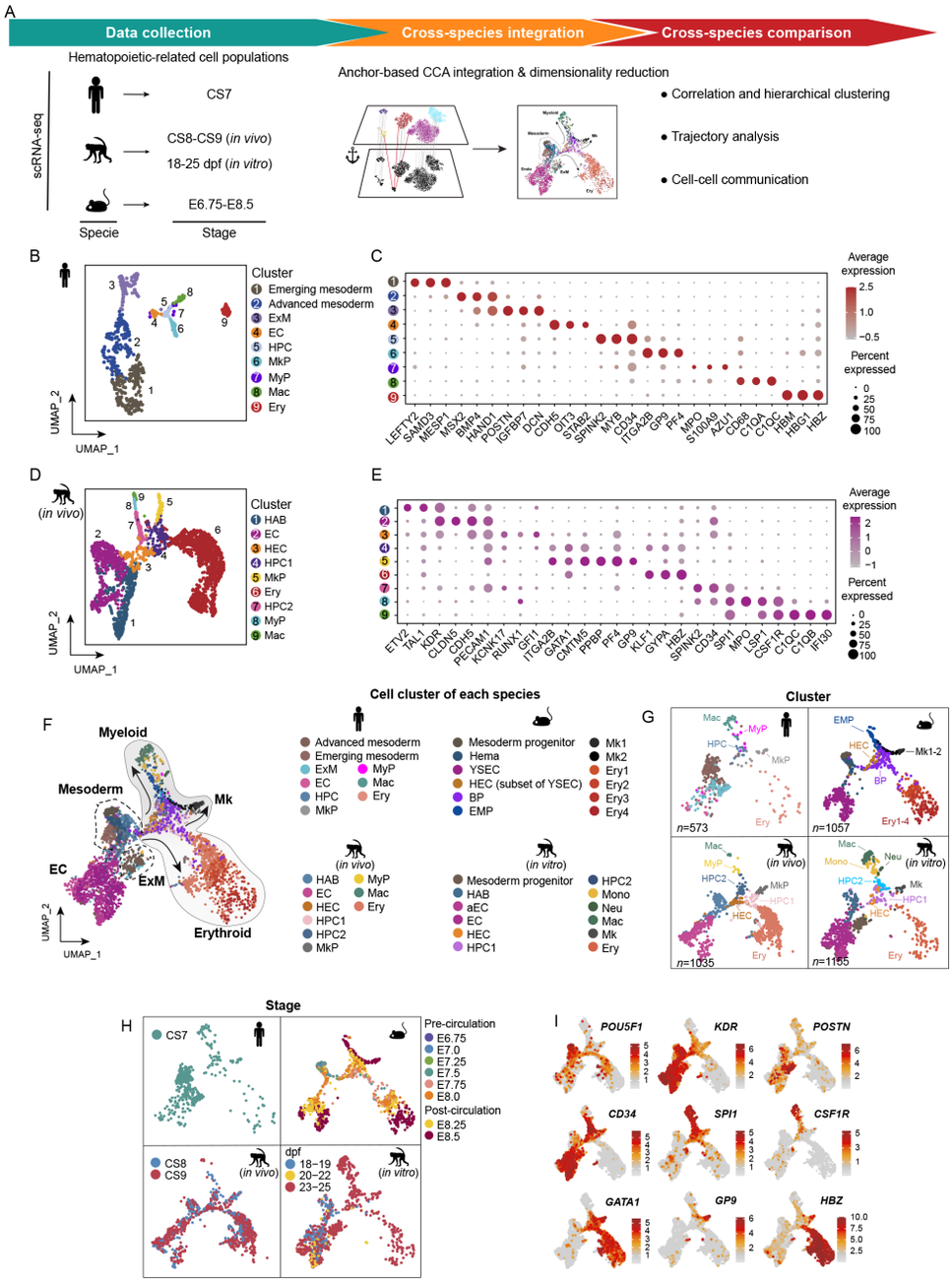


**Figure 1 Construction of transcriptome atlas of pre-circulation hematopoiesis across humans, monkeys, and mice at single-cell resolution**

A: Schematic of cross-species transcriptome integration and comparison of pre-circulation hematopoiesis among humans, monkeys, and mice. CS, Carnegie stage; dpf, days post-fertilization; E, embryonic day; CCA, canonical correlation analysis. B: UMAP visualization of scRNA-seq dataset of hematopoietic-related cells derived from human CS7 embryo. Colors represent cell clusters. ExM, extraembryonic mesoderm; EC, endothelial cell; HPC, hematopoietic progenitor cell; MkP, megakaryocyte progenitor; Ery, erythroblast; MyP, myeloid progenitor; Mac, macrophage. C: Dot plot showing scaled mean expression (color) and proportion of cells expressing genes of cell clusters shown in B from human scRNA-seq dataset. D: UMAP visualization of scRNA-seq dataset of endothelial and hematopoietic-related cells derived from CS8–9 monkey embryos. Colors represent cell clusters. HAB, hemogenic angioblast; HEC, hemogenic endothelial cell. E: Dot plot showing scaled mean expression (color) and proportion (size) of cells expressing genes of cell clusters shown in D from monkey (*in vivo*) scRNA-seq dataset. F: UMAP visualization of integrative cross-species transcriptome atlas of pre-circulation yolk sac hematopoiesis. Colors of each dot represent cell clusters. Four major categories were labeled in UMAP (mesoderm; extraembryonic mesoderm, ExM; endothelial cell, EC; hematopoietic populations, including myeloid, megakaryocytic, and erythroid populations). Cell populations in dashed box are cells related to mesoderm and ExM cells. Cells marked by gray background are hematopoietic populations. Mk, megakaryocytic populations; aEC, arterial endothelial cell; Neu, neutrophil; YSEC, yolk sac endothelial cell; hematopoietic-endothelial progenitor, Hema; BP, blood progenitor; EMP, erythromyeloid progenitor. G: UMAP visualization of cells in F divided by datasets. Colors of each dot represent cell clusters in each dataset and share the same cell annotation in F. H: UMAP visualization of cells in F divided by datasets, dot colors in UMAP represent sampling stages of each cell. I: UMAP visualization showing expression levels of indicated genes in integrated datasets.

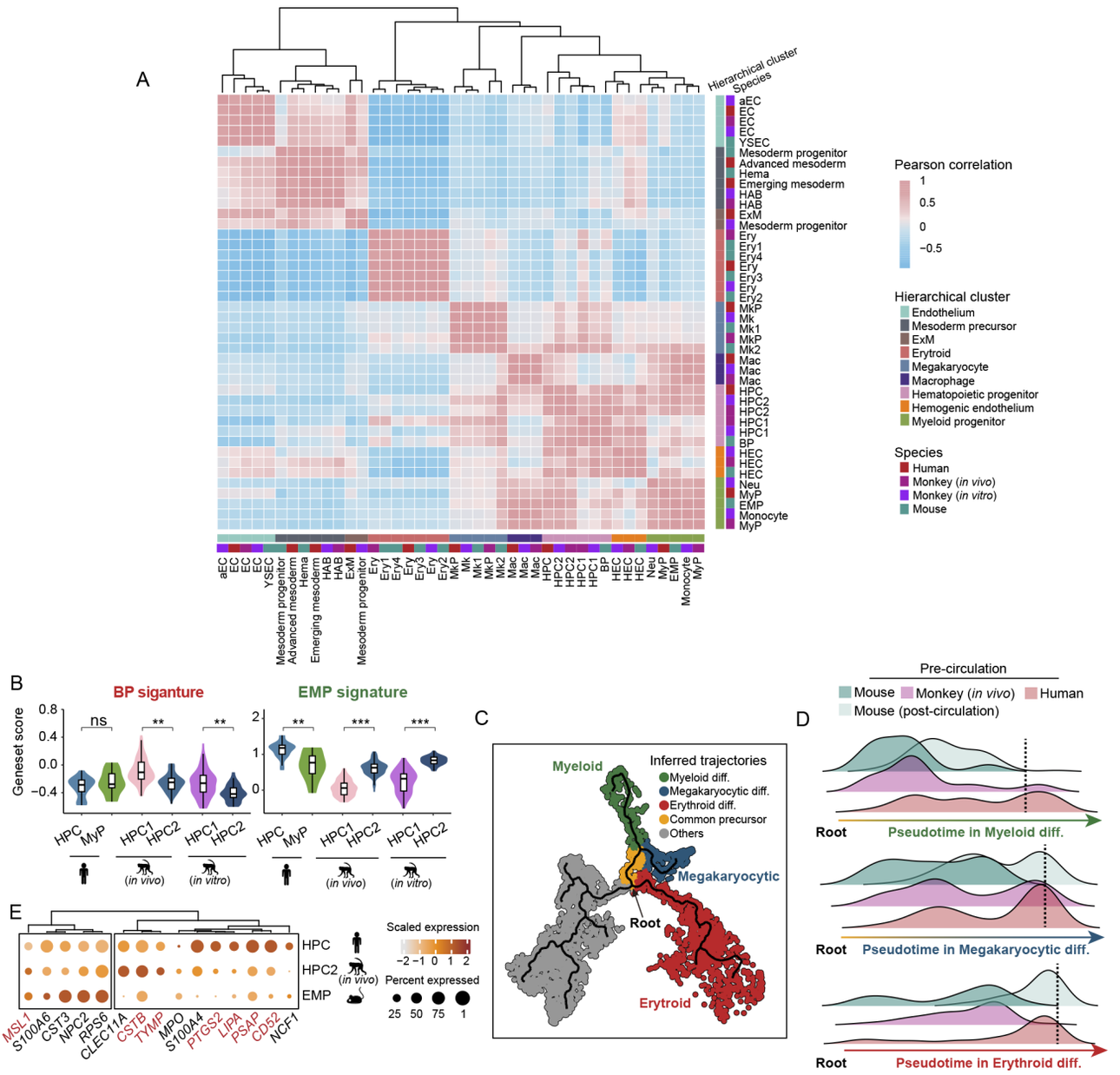


**Figure 2 Cross-species transcriptomic comparison of pre-circulation hematopoiesis**

A: Heatmap visualization of Pearson correlation coefficients between each pair of cell types across datasets from humans, monkeys (*in vivo* and *in vitro*), and mice. Colors represent Pearson correlation coefficients. Hierarchical clustering of cell clusters from integrative cross-species atlas, based on Euclidean distance, is shown on the top of the heatmap. B: Violin plots showing signature scores based on top 60 DEGs between progenitors during the first (BP, left panel) and second (EMP, right panel) hematopoietic wave of the yolk sac in cell clusters from human and monkey datasets. For box plots within each violin plot, center black lines indicate median values, boxes range from the 25th to 75th percentiles. ns: Not significant; **: $P<0.01$; ***: $P<10^{-8}$. C: Pseudotime trajectory showing molecular progression from mesoderm precursors to myeloid (green), megakaryocytic (blue), and erythroid (red) cells (diff. is abbreviation of differentiation). Common precursors (yellow) indicate shared cells in both myeloid and megakaryocytic differentiation. Arrowhead indicates common root point of three hematopoietic trajectories for downstream distribution analysis. D: Ridge plots showing cross-species distribution along pseudotime orders of myeloid (green), megakaryocytic (blue), and erythroid differentiation (red). Colors represent species. While human (CS7) and monkey (CS8–9) datasets were from pre-circulation embryos, the mouse dataset included both pre-circulation (E6.75–E8.0) and post-circulation (E8.25–E8.5) embryos. Dashed lines represent end point of mouse pre-circulation distribution. E: Dot plot showing scaled mean expression (color) and proportion (size) of cells expressing myeloid-related DEGs of human HPC, monkey (*in vivo*) HPC2, and mouse EMP. Pre-macrophage feature genes are labeled in red.

circulation primates compared to mice.

Collectively, integrative analyses of hematopoietic progenitors across species demonstrated that while primates and mice share similar transcriptional signatures, primates exhibit earlier myelopoiesis in pre-circulation hematopoiesis compared to mice (Frame et al., 2016; Palis, 2016).

### *SPP1*$^{+}$ macrophages arise in primates but not in mice before blood circulation onset

Our results indicated a higher degree of myeloid differentiation in primates compared to mice before the onset of blood circulation (Figure 2C, D), with cell clusters expressing the macrophage-specific gene *C1QC* identified in humans and

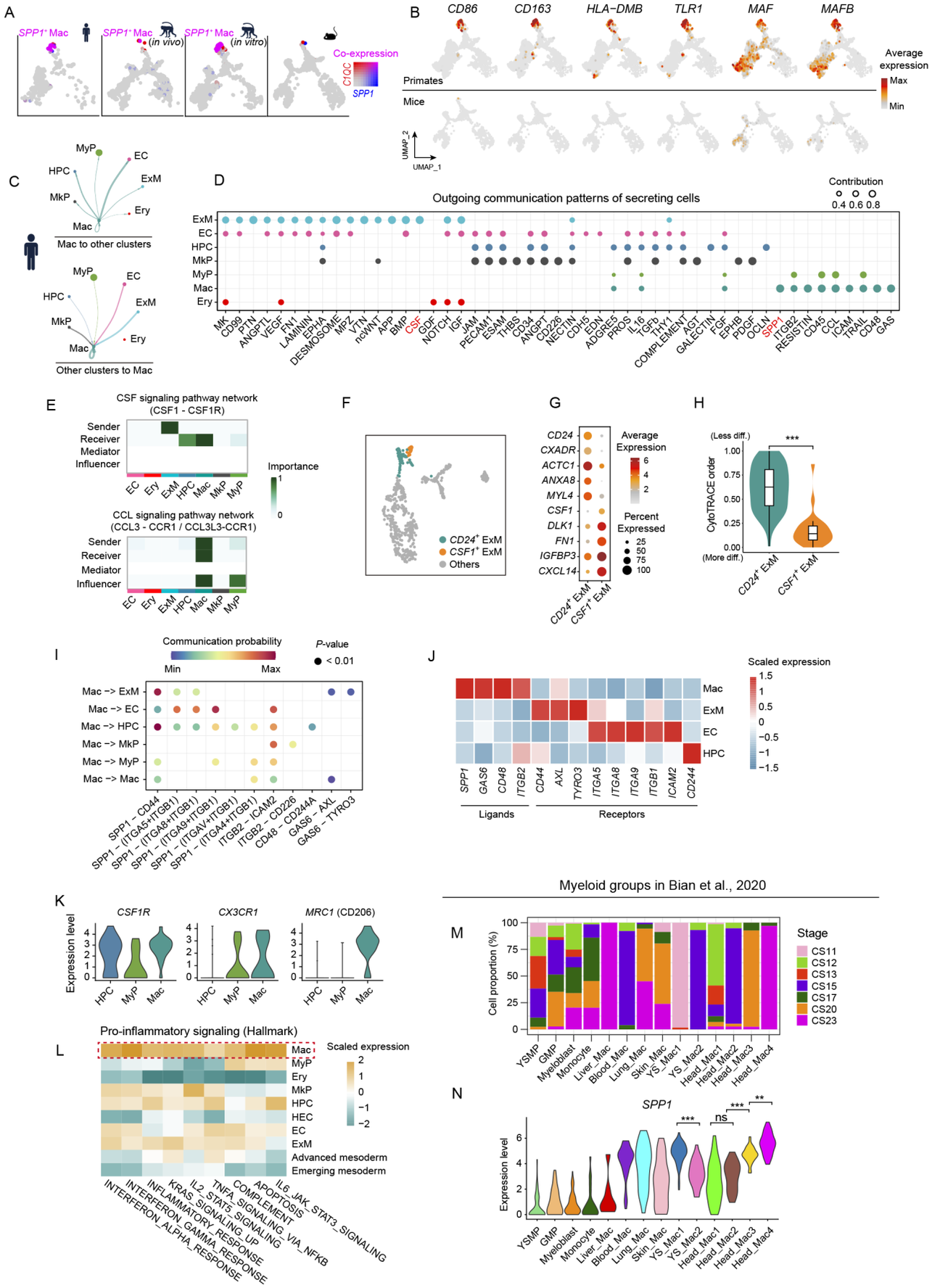
A
SPP1+ Mac
SPP1+ Mac (in vivo)
SPP1+ Mac (in vitro)
Co-expression
C1QC
SPP1
B
CD86
CD163
HLA-DMB
TLR1
MAF
MAFB
Primates
Mice
Average expression
Max
Min
UMAP_2
UMAP_1
C
MyP
EC
HPC
ExM
MkP
Ery
Mac
Mac to other clusters
Other clusters to Mac
D
Outgoing communication patterns of secreting cells
Contribution
0.4 0.6 0.8
ExM
EC
HPC
MkP
MyP
Mac
Ery
MK CD99 PTN ANGPTL VEGF FN1 LAMININ EPHA DESMOSOME MPZ VTN ncWNT APP BMP CSF GDF NOTCH IGF JAM PECAM1 ESAM THBS CD34 ANGPT CD226 NECTIN CDH5 EDN ADGRE5 PROS IL16 TGFb TH1 COMPLEMENT AGT GALECTIN FGF EPHB PDGF OCLN SPP1 ITGB2 RESISTIN CD45 CCL ICAM TRAIL CD48 GAS
E
CSF signaling pathway network
(CSF1 - CSF1R)
Sender
Receiver
Mediator
Influencer
Importance
CCL signaling pathway network
(CCL3 - CCR1 / CCL3L3-CCR1)
F
CD24+ ExM
CSF1+ ExM
Others
G
CD24
CXADR
ACTC1
ANXA8
MYL4
CSF1
DLK1
FN1
IGFBP3
CXCL14
Average Expression
Percent Expressed
25
50
75
100
H
(Less diff.)
(More diff.)
CytoTRACE order
***
I
Communication probability
Min
Max
P-value
< 0.01
Mac -> ExM
Mac -> EC
Mac -> HPC
Mac -> MkP
Mac -> MyP
Mac -> Mac
SPP1 - CD44
SPP1 - (ITGA5+ITGB1)
SPP1 - (ITGA8+ITGB1)
SPP1 - (ITGA9+ITGB1)
SPP1 - (ITGAV+ITGB1)
SPP1 - (ITGA4+ITGB1)
ITGB2 - ICAM2
ITGB2 - CD226
CD48 - CD244A
GAS6 - AXL
GAS6 - TYRO3
J
Scaled expression
Mac
ExM
EC
HPC
SPP1 GAS6 CD48 ITGB2 CD44 AXL TYRO3 ITGA5 ITGA8 ITGA9 ITGB1 ICAM2 CD244
Ligands
Receptors
K
CSF1R
CX3CR1
MRC1 (CD206)
Expression level
HPC
MyP
Mac
L
Pro-inflammatory signaling (Hallmark)
Scaled expression
Mac
MyP
Ery
MkP
HPC
HEC
EC
ExM
Advanced mesoderm
Emerging mesoderm
INTERFERON_ALPHA_RESPONSE
INTERFERON_GAMMA_RESPONSE
INFLAMMATORY_RESPONSE
KRAS_SIGNALING_UP
IL2_STAT5_SIGNALING
TNFA_SIGNALING_VIA_NFKB
COMPLEMENT
APOPTOSIS
IL6_JAK_STAT3_SIGNALING
Myeloid groups in Bian et al., 2020
M
Cell proportion (%)
Stage
CS11
CS12
CS13
CS15
CS17
CS20
CS23
YSMP GMP Myeloblast Monocyte Liver_Mac Blood_Mac Lung_Mac Skin_Mac YS_Mac1 YS_Mac2 Head_Mac1 Head_Mac2 Head_Mac3 Head_Mac4
N
SPP1
Expression level
***
ns
**

**Figure 3 Cell-cell communication analysis of cross-talk between *SPP1*$^+$ Mac and other populations in human yolk sac**

A: UMAP visualization of co-expression levels of *SPP1* and *C1QC* in scRNA-seq datasets of humans, monkeys (*in vivo* and *in vitro*), and mice, respectively. B: UMAP visualization showing comparative view of expression levels of macrophage-related genes (*CD86*, *CD163*, *HLA-DMB*, *TLR1*, *MAF*, and *MAFB*) between primates and mice. C: Network plot showing scaled interaction weight between macrophages and other clusters in human CS7 yolk sac, predicted by CellChat. D: Dot plot showing contribution probability of outgoing ligand-receptor signaling from each human yolk sac cell population in C. Sizes of each dot represent contribution probability, while colors represent cell clusters. E: Heatmap showing importance scores of cell populations from human yolk sac in C contributing to CSF and CCL signaling. In CSF signaling, ExM cells play an exclusive sender role, while macrophages are the major receiver. In CCL signaling, macrophages are the major sender and receiver, indicating a self-regulatory pattern. F: UMAP visualization of the distribution of *CD24*-expressing and *CSF1*-expressing subsets of ExM cells from human yolk sac dataset. Dot colors represent newly defined cell clusters, gray dots other cell populations. G: Dot plot showing average expression (color) and proportion (size) of cells expressing top DEGs between *CD24*$^+$ ExM and *CSF1*$^+$ ExM cells. H: Violin plot showing cell orders ranked by differentiation state (1 to 0 represent less-differentiation to more-differentiation states) predicted by cytoTRACE. For box plots within each violin plot, center black lines indicate median values, boxes range from 25th to 75th percentiles. $^{***}$: $P<10^{-8}$. I: Dot plot showing communication probability (dot color) and *P*-value (dot size) of indicated ligand-receptor interactions between macrophages (sender) and other cell populations (receptor) in C. J: Heatmap visualization of expression levels of ligand and receptor genes in I. K: Violin plot showing expression levels of *CSF1R*, *CX3CR1*, and *MRC1* (encoding CD206) in myeloid-related cell clusters in human dataset. L: Heatmap visualization of expression levels of gene sets related to pro-inflammatory signaling (from Hallmark) in cell clusters from human yolk sac. M: Bar plot showing proportions of sampling stages in each myeloid population from Bian et al. (2020). Macrophages (Mac) were sampled from yolk sac (CS11-CS17), blood (CS13-CS20), liver (CS12-CS23), lung (CS20 and CS23), skin (CS20 and CS23), and head (CS11-CS23). YSMP, yolk sac-derived myeloid-biased progenitor; GMP, granulocyte–monocyte progenitor. N: Violin plot showing expression level of *SPP1* gene in myeloid-related cell clusters in M. Statistical testing was performed between indicated pairs of cell clusters (YS_Mac1 and YS_Mac2, Head_Mac1 and Head_Mac2, Head_Mac2 and Head_Mac3, Head_Mac3 and Head_Mac4). ns: Not significant; $^{**}$: $P<0.01$; $^{***}$: $P<10^{-8}$.

monkeys (*in vivo* and *in vitro*) but not in mice before circulation (Figure 3A). Furthermore, *SPP1*, a marker associated with microglia (Geirsdottir et al., 2019) and pro-fibrotic macrophages in tumor niches (Qi et al., 2022) and lung fibrosis (Morse et al., 2019), was co-expressed with *C1QC* in pre-circulation macrophages of primates but not in mice (Figure 3A). To further characterize the maturity of macrophages identified during hematopoiesis before the onset of blood circulation, we compared the expression levels of commonly recognized macrophage marker genes between primate and mouse datasets. In addition to *CD86* and *CD163*, the human leukocyte antigen (HLA) class II gene *HLA-DMB* and pattern recognition receptor *TLR1*, hallmarks of mature macrophages, were highly expressed in primate macrophages but not in mice (Figure 3B). Furthermore, the transcription factors *MAF* (encoding c-Maf) and *MAFB* (encoding MafB), which regulate the proliferation of differentiated and mature macrophages (Aziz et al., 2009), were also significantly enriched in primate macrophage clusters compared to those in mice (Figure 3A, B). Together with previous research showing that macrophages are not detectable in mice until E8.5–E9.0 (Takahashi et al., 1989), these results suggest the earlier emergence of macrophages in primates relative to mice before the onset of blood circulation.

The above findings raise further questions: what cell compositions within the yolk sac might provide a supportive niche for macrophage generation, and what is the potential role of *SPP1*$^+$ Mac. To explore these questions, we performed cell-cell interaction analysis on the human dataset (Figure 3C). Among the various interactions between *SPP1*$^+$ Mac and other cell populations (Figure 3D), ExM cells emerged as the key contributor to the niche supporting *SPP1*$^+$ Mac (Figure 3C). ExM cells have also been identified as a specific contributor to colony-stimulating factor (CSF) signaling, a crucial pathway regulating macrophage differentiation, proliferation, and survival (Figure 3C–E) (Chitu & Stanley, 2006). Unsupervised clustering further divided ExM cells into *CD24*-expressing and *CSF1*-expressing ExM cells (Figure 3F, G). *CD24*$^+$ ExM cells showed a closer relationship to mesoderm precursors and exhibited a less differentiated state than *CSF1*$^+$ ExM cells (Figure 3F, H). In addition, *CSF1*$^+$ ExM cells showed high expression of *CXCL14*, a chemokine potentially involved in promoting macrophage polarization (He et al., 2023; Tian et al., 2022) (Figure 3G). These results suggest that *CSF1*$^+$ ExM cells likely originate from *CD24*$^+$ ExM cells and provide essential *CSF1* signaling for macrophage development. Moreover, *SPP1*$^+$ Mac may contribute to the supportive niche through self-regulatory mechanisms, particularly via CCL signaling (Figure 3D, E). Next, we investigated the outgoing signaling from *SPP1*$^+$ Mac to speculate on their potential regulatory roles (Figure 3H, I). Multiple interactions were predicted through SPP signaling between Mac and ExM, EC, HPC, and MyP cells (Figure 3C, I). For example, *SPP1*$^+$ Mac interacted with ExM cells and HPC via *CD44*, which was expressed in both cell types. Additionally, *CD48* was exclusively expressed in *SPP1*$^+$ Mac, while its receptor gene, *CD244*, was highly expressed in HPC (Figure 3J), suggesting a potential regulatory role in hematopoiesis.

Emerging evidence has shown that yolk sac-derived myeloid clusters play critical roles in embryonic organogenesis, including regulation of HSC development in the AGM (Mariani et al., 2019; Monticelli et al., 2024). In mice, a subset of yolk sac-derived proinflammatory macrophages migrates to the AGM, where they positively regulate HSC generation (Mariani et al., 2019). However, whether this subset of macrophages is conserved across species remains unclear. To explore this, we assessed key signatures of HSC-regulating macrophages in human *SPP1*$^+$ Mac. In addition to high expression of the chemokine receptor *CX3CR1* and cell surface marker CD206 (encoded by *MRC1*), proinflammatory signaling was also activated in *SPP1*$^+$ Mac (Figure 3K, L). These results suggest that pre-circulation *SPP1*$^+$ Mac in humans resemble proinflammatory AGM macrophages.

To further understand the persistence of pre-circulation macrophages, we evaluated the distribution of *SPP1*$^+$ Mac in later-stage yolk sacs. Based on the expression levels of *SPP1* in myeloid cell populations from previous scRNA-seq data (Figure 3M) (Bian et al., 2020), *SPP1* was found to be highly expressed in most macrophages derived from various

locations compared to myeloid progenitors, such as YSMP and granulocyte–monocyte progenitors (GMP) (Figure 3N). Notably, *SPP1* expression was significantly decreased in yolk sac-derived macrophages from CS11 (YS_Mac1) to CS15 (YS_Mac2), suggesting a potential replacement of pre-circulation SPP1-expressing macrophages by other macrophages in the human yolk sac during the CS11 to CS15 period (Figure 3M, N). Furthermore, *SPP1* expression was detected in macrophages from blood and other tissues, including the brain, lung, and liver (Figure 3N). In the head region, different macrophage subsets (Head_Mac1 to Head_Mac4) emerged in a sequential manner (Figure 3M). In contrast to that in the yolk sac, *SPP1* expression in brain-derived macrophages increased progressively with developmental stage, consistent with its known role as a classical microglia-associated gene (Figure 3N). These findings suggest that *SPP1*$^+$ macrophages in the yolk sac are gradually replaced by other macrophages, while some may migrate to various tissues and organs via the circulation.

In conclusion, we observed the earlier emergence of *SPP1*$^+$ Mac in primates compared to mice, and identified their supporting niche for development, along with potential cross-talk with other components in the human yolk sac.

## DISCUSSION

By constructing an integrative cross-species transcriptome atlas of pre-circulation hematopoiesis in humans, monkeys, and mice, we identified both conserved and divergent features in the early stages of hematopoiesis across these species. Our analysis revealed that primate hematopoietic progenitors shared transcriptomic similarities with the two well-established successive waves of yolk sac hematopoiesis in mice, consistent with the concept that hematopoietic processes are generally conserved among mammals. However, despite the spatiotemporal comparability of HSC emergence in humans and mice (CS14 and E10.5 in the AGM region, respectively) (Calvanese & Mikkola, 2023), there has been limited interspecies comparison of hematopoietic lineage development in the yolk sac prior to HSC formation. Our results highlighted a notable earlier onset of myelopoiesis in pre-circulation primates compared to mice (Figure 4A). Molecular trajectory analysis further demonstrated that myeloid, Mk, and erythroid lineages reached more advanced differentiation states in primates than in mice before the onset of blood circulation. This observation aligns with recent studies suggesting differences in embryonic erythropoiesis between humans and mice (Goh et al., 2023). While such differences

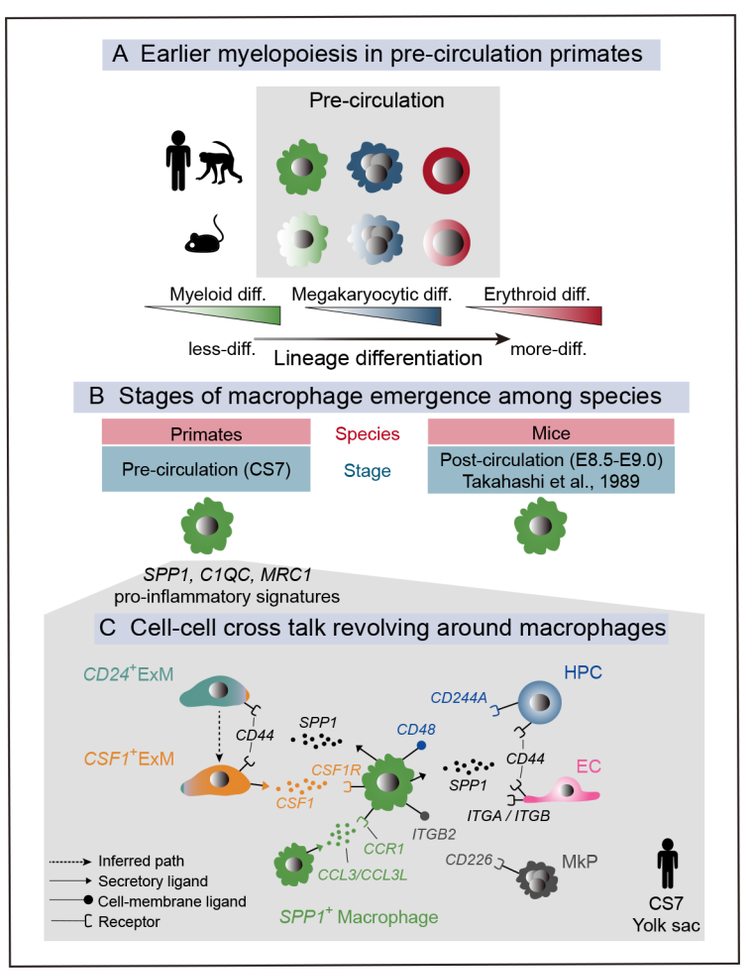


**Figure 4 Schematic showing earlier myelopoiesis and occurrence of macrophages in primates versus mice before blood circulation onset**

A: Gradient of colors in different cell populations, including myeloid, megakaryocyte, and erythroid lineages, showing earlier myelopoiesis in primates compared to mice before blood circulation onset (less-diff. and more-diff. represent less- and more-differentiated states, respectively). B: Earlier occurrence of macrophages in primates but not in mice before blood circulation onset. C: Potential cell-cell cross talk between *SPP1*$^+$ macrophages and other cellular components in human CS7 yolk sac.

may be expected given the distinct developmental patterns of yolk sacs between species (Goh et al., 2023), our findings identified significant discrepancies in early yolk sac hematopoiesis between primates and mice, which warrant careful consideration when selecting animal models for genetic manipulation and functional studies.

Our findings also revealed that *SPP1*-expressing macrophages were detected in primates, but not in mice, before the onset of blood circulation (Figure 4B). Cell-cell interaction analysis suggested that a subset of ExM cells, which exclusively expressed *CSF1*, may provide a supportive niche for macrophage development in the human yolk sac. In contrast, yolk sac-derived macrophages are not detectable in mice until E8.5–E9.0 (Takahashi et al., 1989), raising important questions about the early emergence of *SPP1*$^+$ macrophages in primates, including how pre-circulation macrophages develop so rapidly in primates and what function their early appearance serves.

Regarding the former question, DEG analysis revealed that pre-macrophage signature genes were more highly expressed in human HPC and monkey HPC2 compared to those in mouse EMP. These findings suggest the presence of primate-specific mesoderm progenitors that may give rise to macrophages through a pre-macrophage-dependent “fast track”, consistent with recent studies showing a direct, monocyte-independent trajectory for yolk sac macrophages preceding AGM hematopoiesis (Goh et al., 2023). These results indicate potential cellular, molecular, and developmental pathway differences between primates and mice during pre-circulation hematopoiesis. Regarding the latter question, early-wave HSC-independent macrophages have been increasingly recognized for their regulatory role in organ development (Mariani et al., 2019; Monticelli et al., 2024). We propose that the early emergence of pre-circulation macrophages in primates may serve to meet the early demands of immune function and organogenesis. In addition, the pro-fibrotic role of *SPP1*$^+$ macrophages expressing GAS6-AXL signals suggested a potential contribution to the expansion of the yolk sac by facilitating fibroblast activity (Figure 3H) (Hoeft et al., 2023; Vago et al., 2023). Moreover, putative receptor-ligand interactions in the human yolk sac indicated that pre-circulation macrophages interacted with EC, HPC, and MkP in the human yolk sac (Figure 4C). Interestingly, pre-circulation macrophages in primates exhibited transcriptomic similarities to CD206$^+$ AGM-associated macrophages, which expressed pro-inflammatory signatures that positively regulated HSC generation (Figure 4C) (Mariani et al., 2019). While our analysis confirmed that the transcriptomic profile of HSC-regulating macrophages was conserved between primates and mice, the specific *in vivo* function of these macrophages in primates requires further exploration and validation. In addition to their origin, the *in vivo* fate of *SPP1*-expressing macrophages is also of interest. Analysis of *SPP1* expression in late yolk sac myeloid populations showed that *SPP1* remained highly expressed in yolk sac macrophages at CS11 but declined significantly by CS15. *SPP1* expression in macrophages derived from circulating blood and other organs, such as brain and lung, suggested that *SPP1*$^+$ macrophages may colonize other organs through blood circulation.

In conclusion, our integrative analysis highlighted critical cross-species differences in pre-circulation hematopoiesis between primates and mice. Our cross-species comparison not only provides valuable insights into human pre-circulation yolk sac hematopoiesis but also facilitates optimization of the selection of appropriate animal models for genetic manipulation and functional validation. This study will help to understand the theoretical basis for the regeneration of functional blood cells, especially macrophages.

## LIMITATIONS

There are several limitations in this study. First, the human dataset was relatively small, derived from a single embryo at a single time point (CS7), which may introduce individual bias. For instance, the absence of an erythroid-biased hematopoietic progenitor cluster in the human CS7 dataset could be attributed to the small size of the dataset. To address this issue in future research, it will be necessary to include additional replicates spanning broader time points to validate key findings in pre-circulation hematopoiesis, especially given the significant heterogeneity in humans. Furthermore, the *in vivo* origin of pre-circulation macrophages in primates remains unclear and requires further investigation using lineage-tracing techniques. While these tools are widely used in mice, their application in primates is currently challenging and lacks the efficiency needed for comprehensive studies. Advances in these technologies will help shed light on the earliest stages of hematopoiesis in humans.

## COMPETING INTERESTS

The authors declare that they have no competing interests.

## AUTHORS’ CONTRIBUTIONS

Y.L. and B.L. conceived and designed the study; J.D., Z.L., and Y.G. performed data collection, bioinformatics analysis, and data visualization; J.D., Z.L., and Y.G. wrote the manuscript. All authors reviewed the manuscript. All authors read and approved the final version of the manuscript.

## ACKNOWLEDGMENTS

The authors are grateful to Dr. Di Liu (Peking University) and Dr. Guoju You (Tsinghua University) for their technical assistance in this work.

## REFERENCES

Aziz A, Soucie E, Sarrazin S, et al. 2009. MafB/c-Maf deficiency enables self-renewal of differentiated functional macrophages. *Science*, **326**(5954): 867–871.

Bian ZL, Gong YD, Huang T, et al. 2020. Deciphering human macrophage development at single-cell resolution. *Nature*, **582**(7813): 571–576.

Calvanese V, Capellera-Garcia S, Ma FY, et al. 2022. Mapping human haematopoietic stem cells from haemogenic endothelium to birth. *Nature*, **604**(7906): 534–540.

Calvanese V, Mikkola HKA. 2023. The genesis of human hematopoietic stem cells. *Blood*, **142**(6): 519–532.

Canu G, Ruhrberg C. 2021. First blood: the endothelial origins of hematopoietic progenitors. *Angiogenesis*, **24**(2): 199–211.

Cao JY, Spielmann M, Qiu XJ, et al. 2019. The single-cell transcriptional landscape of mammalian organogenesis. *Nature*, **566**(7745): 496–502.

Chitu V, Stanley ER. 2006. Colony-stimulating factor-1 in immunity and inflammation. *Current Opinion in Immunology*, **18**(1): 39–48.

Durinck S, Spellman PT, Birney E, et al. 2009. Mapping identifiers for the integration of genomic datasets with the R/Bioconductor package biomaRt. *Nature Protocols*, **4**(8): 1184–1191.

Dzierzak E, Bigas A. 2018. Blood development: hematopoietic stem cell dependence and independence. *Cell Stem Cell*, **22**(5): 639–651.

Frame JM, Fegan KH, Conway SJ, et al. 2016. Definitive hematopoiesis in the yolk sac emerges from wnt-responsive hemogenic endothelium independently of circulation and arterial identity. *Stem Cells*, **34**(2): 431–444.

Geirsdottir L, David E, Keren-Shaul H, et al. 2019. Cross-species single-cell analysis reveals divergence of the primate microglia program. *Cell*, **179**(7): 1609–1622. e16.

Ginhoux F, Greter M, Leboeuf M, et al. 2010. Fate mapping analysis reveals that adult microglia derive from primitive macrophages. *Science*, **330**(6005): 841–845.

Goh I, Botting RA, Rose A, et al. 2023. Yolk sac cell atlas reveals multiorgan functions during human early development. *Science*, **381**(6659): eadd7564.

Gong YD, Bai B, Sun NQ, et al. 2023. *Ex utero* monkey embryogenesis from blastocyst to early organogenesis. *Cell*, **186**(10): 2092–2110. e23.

Gulati GS, Sikandar SS, Wesche DJ, et al. 2020. Single-cell transcriptional diversity is a hallmark of developmental potential. *Science*, **367**(6476): 405–411.

Hänzelmann S, Castelo R, Guinney J. 2013. GSVA: gene set variation analysis for microarray and RNA-seq data. *BMC Bioinformatics*, **14**(1): 7.

Hao YH, Hao S, Andersen-Nissen E, et al. 2021. Integrated analysis of multimodal single-cell data. *Cell*, **184**(13): 3573–3587. e29.

He PK, Wang H, Cheng SB, et al. 2023. Geniposide ameliorates atherosclerosis by regulating macrophage polarization via perivascular adipocyte-derived CXCL14. *Journal of Ethnopharmacology*, **314**: 116532.

Hoeft K, Schaefer GJL, Kim H, et al. 2023. Platelet-instructed SPP1$^{+}$ macrophages drive myofibroblast activation in fibrosis in a CXCL4-dependent manner. *Cell Reports*, **42**(2): 112131.

Jin SQ, Guerrero-Juarez CF, Zhang LH, et al. 2021. Inference and analysis of cell-cell communication using CellChat. *Nature Communications*, **12**(1): 1088.

Li ZH, Dulyaninova NG, House RP, et al. 2010. S100A4 regulates macrophage chemotaxis. *Molecular Biology of the Cell*, **21**(15): 2598–2610.

Mariani SA, Li Z, Rice S, et al. 2019. Pro-inflammatory aorta-associated macrophages are involved in embryonic development of hematopoietic stem cells. *Immunity*, **50**(6): 1439–1452. e5.

Mass E, Ballesteros I, Farlik M, et al. 2016. Specification of tissue-resident macrophages during organogenesis. *Science*, **353**(6304): aaf4238.

Medvinsky A, Dzierzak E. 1996. Definitive hematopoiesis is autonomously initiated by the AGM region. *Cell*, **86**(6): 897–906.

Monticelli S, Sommer A, Alhajj Hassan Z, et al. 2024. Early-wave macrophages control late hematopoiesis. *Developmental Cell*, **59**(10): 1284–1301. e8.

Morse C, Tabib T, Sembrat J, et al. 2019. Proliferating SPP1/MERTK-expressing macrophages in idiopathic pulmonary fibrosis. *European Respiratory Journal*, **54**(2): 1802441.

Neo WH, Lie-A-Ling M, Fadlullah MZH, et al. 2021. Contributions of embryonic HSC-independent hematopoiesis to organogenesis and the adult hematopoietic system. *Frontiers in Cell and Developmental Biology*, **9**: 631699.

Palis J. 2016. Hematopoietic stem cell-independent hematopoiesis: emergence of erythroid, megakaryocyte, and myeloid potential in the mammalian embryo. *FEBS Letters*, **590**(22): 3965–3974.

Palis J, Malik J, Mcgrath KE, et al. 2010. Primitive erythropoiesis in the mammalian embryo. *The International Journal of Developmental Biology*, **54**(6-7): 1011–1018.

Peschle C, Migliaccio AR, Migliaccio G, et al. 1984. Embryonic----Fetal Hb switch in humans: studies on erythroid bursts generated by embryonic progenitors from yolk sac and liver. *Proceedings of the National Academy of Sciences of the United States of America*, **81**(8): 2416–2420.

Picelli S, Faridani OR, Björklund ÅK, et al. 2014. Full-length RNA-seq from single cells using Smart-seq2. *Nature Protocols*, **9**(1): 171–181.

Pijuan-Sala B, Griffiths JA, Guibentif C, et al. 2019. A single-cell molecular map of mouse gastrulation and early organogenesis. *Nature*, **566**(7745): 490–495.

Qi JJ, Sun HX, Zhang Y, et al. 2022. Single-cell and spatial analysis reveal interaction of *FAP*$^{+}$ fibroblasts and *SPP1*$^{+}$ macrophages in colorectal cancer. *Nature Communications*, **13**(1): 1742.

Ross C, Boroviak TE. 2020. Origin and function of the yolk sac in primate embryogenesis. *Nature Communications*, **11**(1): 3760.

Takahashi K, Yamamura F, Naito M. 1989. Differentiation, maturation, and proliferation of macrophages in the mouse yolk sac: a light-microscopic, enzyme-cytochemical, immunohistochemical, and ultrastructural study. *Journal of Leukocyte Biology*, **45**(2): 87–96.

Tian HY, Liang Q, Shi Z, et al. 2022. Exosomal CXCL14 contributes to M2 macrophage polarization through NF-$\kappa$B signaling in prostate cancer. *Oxidative Medicine and Cellular Longevity*, **2022**: 7616696.

Tyser RCV, Mahammadov E, Nakanoh S, et al. 2021. Single-cell transcriptomic characterization of a gastrulating human embryo. *Nature*, **600**(7888): 285–289.

Vago JP, Valdrighi N, Blaney-Davidson EN, et al. 2023. Gas6/Axl axis activation dampens the inflammatory response in osteoarthritic fibroblast-like synoviocytes and synovial explants. *Pharmaceuticals*, **16**(5): 703.

Wang CJ, Gong YD, Wei AB, et al. 2021. Adult-repopulating lymphoid potential of yolk sac blood vessels is not confined to arterial endothelial cells. *Science China Life Sciences*, **64**(12): 2073–2087.

Zhai JL, Guo J, Wan HF, et al. 2022. Primate gastrulation and early organogenesis at single-cell resolution. *Nature*, **612**(7941): 732–738.

Zhang X, Lai GY, Volpe G, et al. 2022. Towards a primate single-cell atlas. *Zoological Research*, **43**(4): 691–694.